JMEPEG (2012) 21:660–666
DOI: 10.1007/s11665-012-0127-1

1059-9495/$19.00

Control of Interfacial Reactivity Between ZrB_2 and Ni-Based Brazing Alloys

F. Valenza, M.L. Muolo, A. Passerone, G. Cacciamani, and C. Artini

(Submitted December 26, 2011)

Transition metals diborides $(Ti,Zr,Hf)B_2$ play a key role in applications where stability at extremely high temperatures and damage tolerance are required; however, much research has still to be done to optimize the joining of these materials to themselves or to other high-temperature materials. In this study, the reactivity at the solid-liquid interface between ZrB_2 ceramics and Ni-based brazing alloys has been addressed; it is shown how the reactivity and the dissolution of the solid phase can be controlled and even suppressed by adjusting the brazing alloy composition on the basis of thermodynamic calculations. Wetting experiments on ZrB_2 ceramics by Ni, Ni-B 17 at.%, and Ni-B 50 at.% were performed at 1500 and 1200 °C by the sessile drop technique. The obtained interfaces were characterized by optical microscopy and SEM-EDS, and interpreted by means of the ad hoc-calculated B-Ni-Zr ternary diagram. A correlation among microstructures, substrate dissolution, shape of the drops, spreading kinetics, and the phase diagram was found. The effect on the interfacial reactivity of Si_3Ni_4 used as a sintering aid and issues related to Si diffusion into the brazing alloy are discussed as well.

Keywords borides, brazing, CALPHAD, wetting

1. Introduction

Transition-metal diborides are ceramic materials with an attractive combination of properties: extremely high melting temperature, high hardness and chemical inertness, high thermal and electrical conductivities, and thermal shock resistance (Ref 1-3). In order to support the exigent operating conditions targeted by these materials, such as high thermal fluxes and severe surface stresses, it is necessary to design specific processes for joining ceramics to other ceramics or to special alloys. Joints must be reliable, robust, and the methods of joining must become increasingly capable of successfully accommodating new materials combinations and fabricating structures with an increasing geometric complexity and size.

When using liquid-phase-bonding processes, understanding how well the liquid wets the two solid surfaces, investigating the interplay between liquid and solid chemistries and the interfacial energetics, and controlling the interfacial reactions are essential to develop new joining approaches.

Some data addressing these issues are already available in the literature for transition-metal diborides since 1970s (Ref 4-8). In the recent years, more articles appeared on this topic fueled by a renewed interest for these materials. A broad survey of the results for diborides of the metals belonging to the IV Group (Ti, Zr, and Hf) can be found in Passerone et al. (Ref 9, 10) and in Muolo et al. (Ref 11). On top of the wetting studies, many articles appeared in the last ten years describing joining processes or metal- ceramic composite formation especially for TiB_2 (Ref 12-15) and ZrB_2 (Ref 16-23), while just a few studies involve HfB_2 (Ref 11, 24).

In particular, this author group has undertaken a systematic study on wettability, reactivity, and interfacial properties of diborides belonging to the IV Group (Ti, Zr, and Hf). Such kind of studies are carried out by the sessile drop method (Ref 9, 25-27), and the experimental findings are interpreted and supported from the basic point of view by multi-component phase diagrams calculated by the CALPHAD method (Ref 28-30) or by first-principle approaches, such as the Density Functional Theory (Ref 31).

Within this framework, in this article, the wettings of ZrB_2 by Ni and two binary Ni-B alloys were evaluated by means of the sessile drop method at 1500 and 1200 °C. The composition of the alloys were Ni/17 at.% B (NiB17), that is, the eutectic composition having melting point at 1093 °C and Ni/50 at.% B (NiB50), that is, the intermetallic compound with a peritectic reaction at 1035 °C. After tests, the obtained interfaces were characterized by optical microscopy and SEM-EDS.

A more in-depth understanding of the behavior of these systems is presented on the basis of the newly computed B-Ni-Zr ternary phase diagram (Ref 28) which integrates the scant existing literature data based on two isothermal sections, namely, at 800 °C (Ref 32) and 850 °C (Ref 33), and on the partial vertical section between pure Ni and $Zr_2Ni_{21}B_6$ (Ref 34).

This article is an invited submission to JMEP selected from presentations at the Symposia "Wetting, soldering and brazing" and "Diffusion bonding and characterization" belonging to the Topic "Joining" at the European Congress and Exhibition on Advanced Materials and Processes (EUROMAT 2011), held September 12-15, 2011, in Montpellier, France, and has been expanded from the original presentation.

F. Valenza, M.L. Muolo, A. Passerone, and **C. Artini**, National Research Council-Institute for Energetics and Interphases (CNR-IENI), Genoa, Italy; and **G. Cacciamani**, Department of Chemistry and Industrial Chemistry (DCCI), University of Genova, Genoa, Italy. Contact e-mail: valenza@ge.ieni.cnr.it.

The complete new set of data allows a more reliable interpretation of the solid-liquid interaction phenomena observed during wetting experiments; on the other hand, the prediction of the interfacial behavior of the metal-ceramic system can assist the formulation of new alloy compositions.

The effects on the interfacial reactivity of Si_3Ni_4 used as a sintering enhancer to improve the final density and microstructure of ZrB_2, and issues related to Si diffusion into the brazing alloy are discussed as well.

2. Materials and Experimental

2.1 Materials

The ZrB_2 specimens used in this study were produced by ISTEC-CNR (Faenza, I), as described by Monteverde et al. (Ref 35), by the hot isostatic pressing technique. Si_3N_4 was added (5 vol.%) to the starting ZrB_2 powder to act as a sintering enhancer. The heating rate to the final temperature of 1700 °C was 900 °C/h and the soaking time was 15 min; during the process, a pressure of 30 MPa was applied. The final density of the sintered ceramic is 5.86×10^3 kg/m^3, which corresponds to a relative density of 0.98.

Before testing, the substrates were polished on diamond grinding disks to reach a final surface roughness R_a = 0.03 μm measured over a length of 4.8 mm.

The NiB17 alloy has been prepared by pre-melting the pure Ni (>99.99%; Goodfellow, Cambridge, UK) and crystalline powder B (>99.4%; size <180 μm; H.C. Starck, Goslar, D) in alumina crucibles under high-vacuum conditions ($P = 10^{-4}$ Pa) in the presence of a Zr getter. The NiB50 alloy was prepared under the same conditions starting from an alloy precursor (>99.8%; Goodfellow, Cambridge, UK) in the form of powder with a maximum particle size of 150 μm.

The final morphology and composition of the alloys were checked using electron microscopy (SEM) coupled with energy-dispersive spectroscopy (EDS) analysis. Pieces of about 0.3 g of these alloys were then mechanically and chemically cleaned and used for the sessile drop tests.

2.2 Experimental

Wetting was evaluated by measurement of contact angle and drop dimensions (height and base diameter) measurements using the sessile drop technique (Ref 36) and the ad hoc-designed ASTRAView image analysis software, which allows obtained by surface tension, drop dimensions, and contact angle data (θ) during each experimental run (Ref 37).

The experimental apparatus for wetting tests consists of a specially designed furnace which can reach 1600 °C; the experimental chamber is made of two concentric, horizontal alumina tubes connected to a high-vacuum system; the apparatus has been fully described in a previous publication (Ref 38). The metal/ceramic couples were introduced into the preheated furnace by a magnetically operated push rod only after all parameters (temperature T, oxygen partial pressure PO_2, etc.) had reached equilibrium; complete melting occurred in ~30 s. After the tests, the samples were taken out from the hot zone and allowed to cool down without opening the furnace.

Experiments were performed at 1500 °C for all the compositions, while NiB17 and NiB50, which melt at lower temperatures, were tested at 1200 °C as well. An Ar + 5 at% H_2 mixture was used as a testing atmosphere with a flow of 0.001 l/s (measured at STP); the PO_2 of the working atmosphere was continuously monitored by solid-state oxygen sensors at the chamber's inlet and outlet. In this study, Zr getters surrounded the specimens, which should set a theoretical minimum PO_2 of 10^{-18} Pa or 10^{-23} Pa, i.e., the equilibrium dissociation pressures of ZrO_2 at 1500 and 1200 °C, respectively.

The drop/substrate couples were recorded as sharp, back-lit images, using a high-resolution CCD camera. The drop dimensions could be calculated with a precision of ±1 μm through a careful determination of the magnification factor, while the intrinsic precision of contact angle data is of the order of ±0.5°; however, possible optical distortions due to the high temperature involved lead to uncertainties in the measured profiles, suggesting a more conservative final contact angle accuracy of the order of ±2° (Ref 39).

The samples were held at high temperature for 1800 s; after the tests, the top surface of the drops was observed and analyzed by optical and SEM/EDS analysis, as well as the metal-ceramic interfaces after cross-sectioning of the samples.

3. Results and Discussion

3.1 Wetting at 1500 °C

Wettability data are summarized in Table 1; for all the systems analyzed in this study, a condition of wetting (θ < 90°) is achieved. As described in the following, since the metal-ceramic couples underwent strong interfacial interactions, the final contact angles reported here are "apparent angles" as they are a measure of that part of the angle above the solid surface without taking into account the hidden part below it.

At 1500 °C, pure Ni wets ZrB_2 according to the spreading kinetics shown in Fig. 1. Three steps can be recognized: (a) a first spreading immediately after the melting of the metal; (b) a stationary stage lasting about 500 s with a constant contact angle of ~23°; and (c) a further spreading with a final contact angle of less than 10°. For the NiB17 alloy, a similar spreading kinetics is reported, and the final contact angle is less than 10° as well.

For the NiB50 alloy, after the spreading, which takes place in about 25 s, no further evolution occurs, and the final contact angle is 30°.

The cross sections of the three couples, namely Ni/ZrB_2, NiB17/ZrB_2, and NiB50/ZrB_2 after the test at 1500 °C, are shown in Fig. 2. A remarkable substrate dissolution is clearly visible at the solid/liquid interface in the Ni/ZrB_2 cross section, and a sigmoidal profile of the interface is formed. The same phenomenon, even if less pronounced, can be observed in the case of NiB17, while it is suppressed for NiB50.

Comparisons between the drop base diameters measured during the wetting tests and on the cross-sectioned samples let us infer that the dimensions of the central crater, formed by

Table 1 Summary of the final contact angles

	Pure Ni, °	NiB17, °	NiB50, °
1500 °C	<10	<10	30
1200 °C	…	21	58

dissolution, correspond to the base diameters measured at the end of step (a) of Fig. 1. Then, during the stationary stage (step b), further spreading is limited by the pinning of the drop at the triple line. Subsequently (step c), the de-pinning causes the spreading of the newly formed B-Ni-Zr ternary alloy over the ceramic surface to reach the final situation shown in the cross-sectional images. Therefore, the sigmoidal profile of the interface is the result of the interplay between dissolution and further spreading of the saturated alloy. The dissolution of the ceramic substrate results due to the introduction into the melt of its constituents that are, besides B and Zr, the Si-compounds formed from Si_3N_4 used as a sintering enhancer.

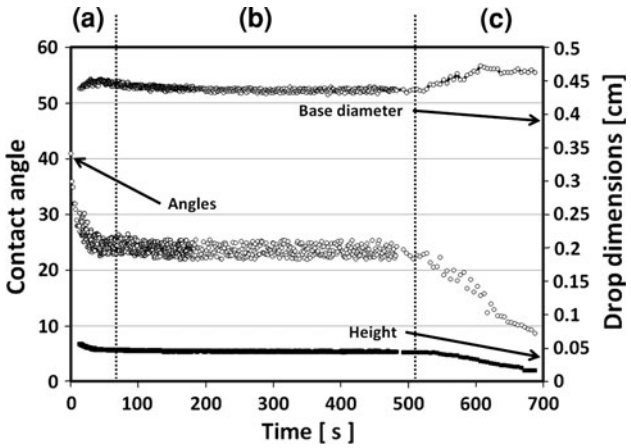

Fig. 1 Contact angle and drop dimensions for the Ni/ZrB_2 sample. Dotted lines delimit the steps of the wetting kinetics: (a) initial spreading; (b) stationary stage; (c) final spreading

Optical and SEM micrographs reveal that on the top of the Ni and NiB17 solidified drops, hexagonal crystals can be found with composition ZrB_2 (Fig. 3), while NiB50-solidified drop shows recrystallized ZrB_2 in a considerably smaller amount. Both the shape and the dimension of these crystals, which are different from those of the as-received ceramic, prove that they form from the primary solidification of the melt.

Analyses of the cross sections of the solidified drops do not show the presence of any ZrB_2 crystal in the interior, because the density of ZrB_2 (6.09×10^3 kg/m^3) is lower than the one of the liquid quaternary B-Ni-Si-Zr alloy. Moreover, smaller ZrB_2 crystals can also be found around the solidified drop, close the triple line, meaning that, during cooling, a shrinkage of the drop takes place, which leaves behind ZrB_2 crystals and does not allow them to grow like the ones on the top.

The compositions of the bulk alloys after solidification reflect the situation described so far. For the pure Ni/ZrB_2 system, the final microstructure is shown in Fig. 4. An eutectic structure was formed upon solidification which is constituted

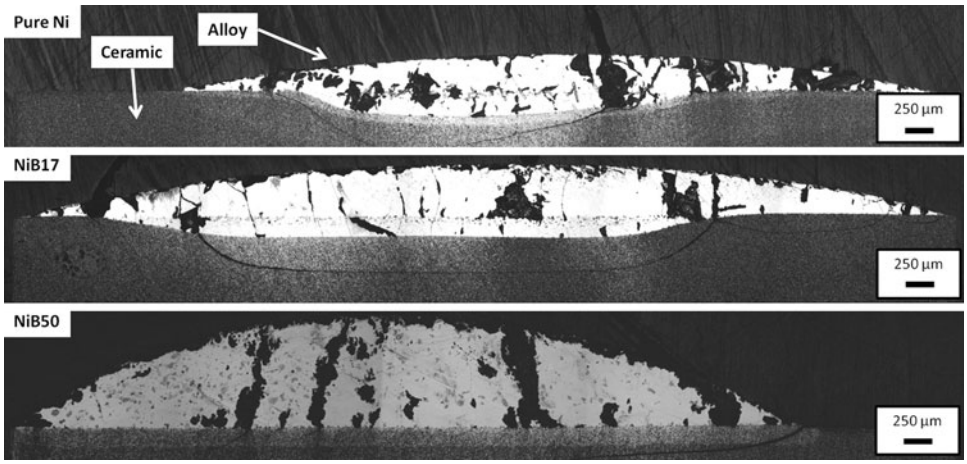

Fig. 2 Optical microscope (OM) pictures of the cross sections of the Ni/ZrB_2, NiB17/ZrB_2 and NiB50/ZrB_2 samples after test at 1500 °C

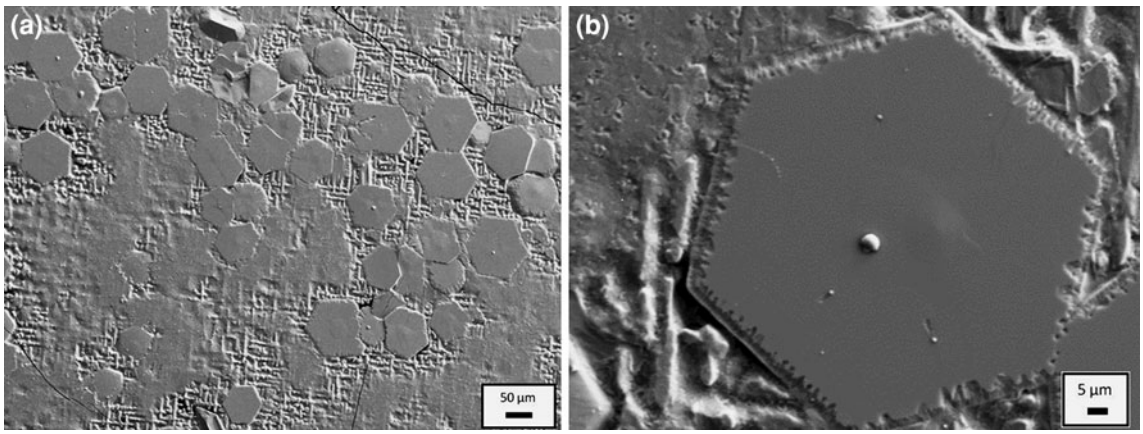

Fig. 3 SEM pictures (secondary electron—SE mode) of hexagonal crystals of ZrB_2 formed by recrystallization during cooling

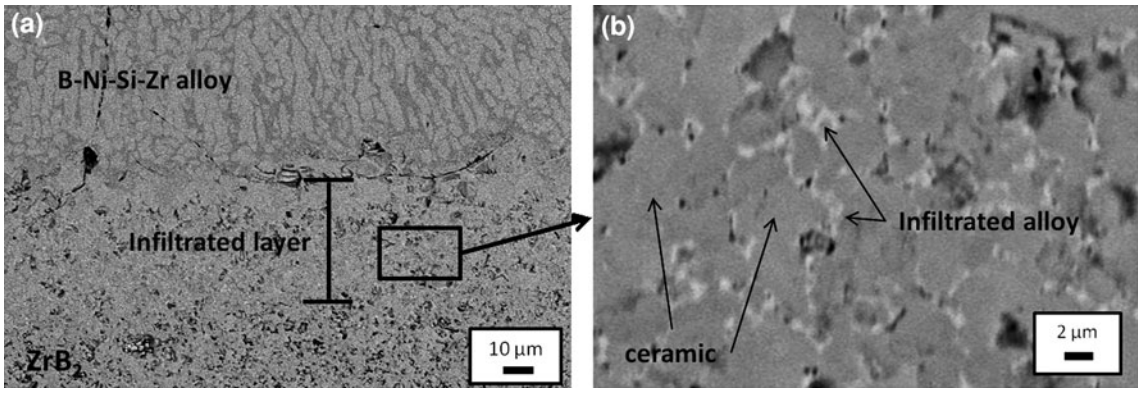

Fig. 4 SEM pictures (back-scattered electrons—BSE mode) of the cross section of a pure Ni/ZrB_2 sample. Left: from top to bottom: solidified alloy, infiltrated layer, ZrB_2 substrate. Right: high magnification of the infiltrated layer

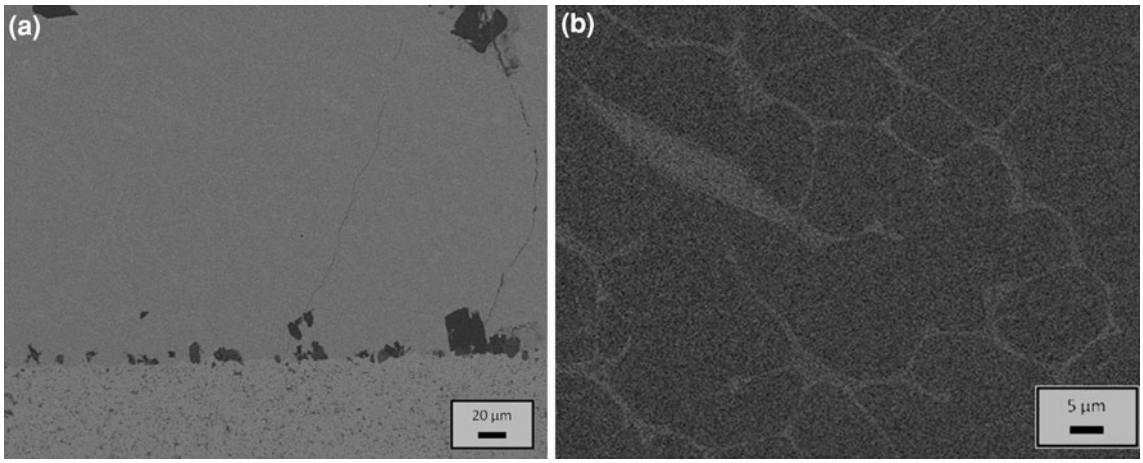

Fig. 5 SEM pictures (BSE mode) of the cross section of a NiB50/ZrB_2 sample: (a) overview of the interfacial area with boron precipitates (black spots); (b) solidification structure of the alloy; dark zones: original NiB alloy, bright zones: Ni-B-Zr-Si alloy

by a phase, bright in the picture, containing Ni, B, and Zr in proportions similar to the compound $Zr_2Ni_{21}B_6$; and a zone (dark) containing, besides Ni and B, up to 20 at.% of Si with a negligible amount of Zr (<2 at.%). During the process, the liquid alloy infiltrates into the ceramic pores leaving under the drop a metal/ceramic layer with thickness of about 40 µm as is clearly visible in Fig. 4.

A similar situation is reported for the NiB17 alloy, but the dissolution of the substrate is less marked; again, an eutectic structure forms, constituted by the $Zr_2Ni_{21}B_6$ compound and a B, Ni, and Si alloy.

The cross section of the solidified NiB50 drop shows an interface which remained macroscopically planar, indicating that the dissolution took place only to a limited extent. Microanalysis revealed the presence of boron crystals, mainly at the metal-ceramic interface, formed during cooling (Fig. 5a) and the absence of the $Zr_2Ni_{21}B_6$ compound. The bulk phase is mainly constituted by a Ni-B alloy, while the presence of Si is limited to the bright zones shown in Fig. 5(b). The low amount of Zr derived from the slight dissolution forms, upon cooling, the ZrB_2 crystals found on the top of the drop.

Phenomena observed during wetting tests as well as in micrographs and EDS analyses can be explained on the basis of the Ni-B-Zr phase diagram (Fig. 6): when the molten alloys are brought into contact with ZrB_2 at a certain temperature, an equilibrium condition is established between the two phases, which can be followed on the corresponding isothermal section. On the basis of the computed phase diagram (Fig. 6a), pure Ni, when placed in contact with ZrB_2, melts at a temperature (about 1100 °C) well below its melting point (1453 °C), giving rise to a ternary liquid phase due to an important dissolution of ZrB_2. The isothermal section at 1500 °C of the ternary diagram (Fig. 6c) shows also that, at the same temperature, the dissolution of the boride is greatly reduced and almost disappears if a Ni-B alloy with $X_B > 50$ at.% is placed in contact with ZrB_2.

Indeed, pure Ni in contact with ZrB_2 enters a biphasic equilibrium formed by a solid (ZrB_2) and a liquid phase with composition indicated by point α. An increased amount of B in the alloy causes a reduction in the ZrB_2 dissolution and a variation of the liquid phase composition, which follows the liquidus line from point α through point β to γ for Ni, NiB17, and NiB50. The reduced substrate dissolution with increasing B content explains the gradual disappearance of the sigmoidal shape of the interface previously described.

On lowering temperature, the ZrB_2/liquid biphasic region of the Ni-ZrB_2 isopleth widens, the concentration of Ni in the liquid increases, and, at the same time, the recrystallization of a certain amount of ZrB_2 takes place. The extent of this phenomenon decreases from Ni to NiB17 to NiB50, as the

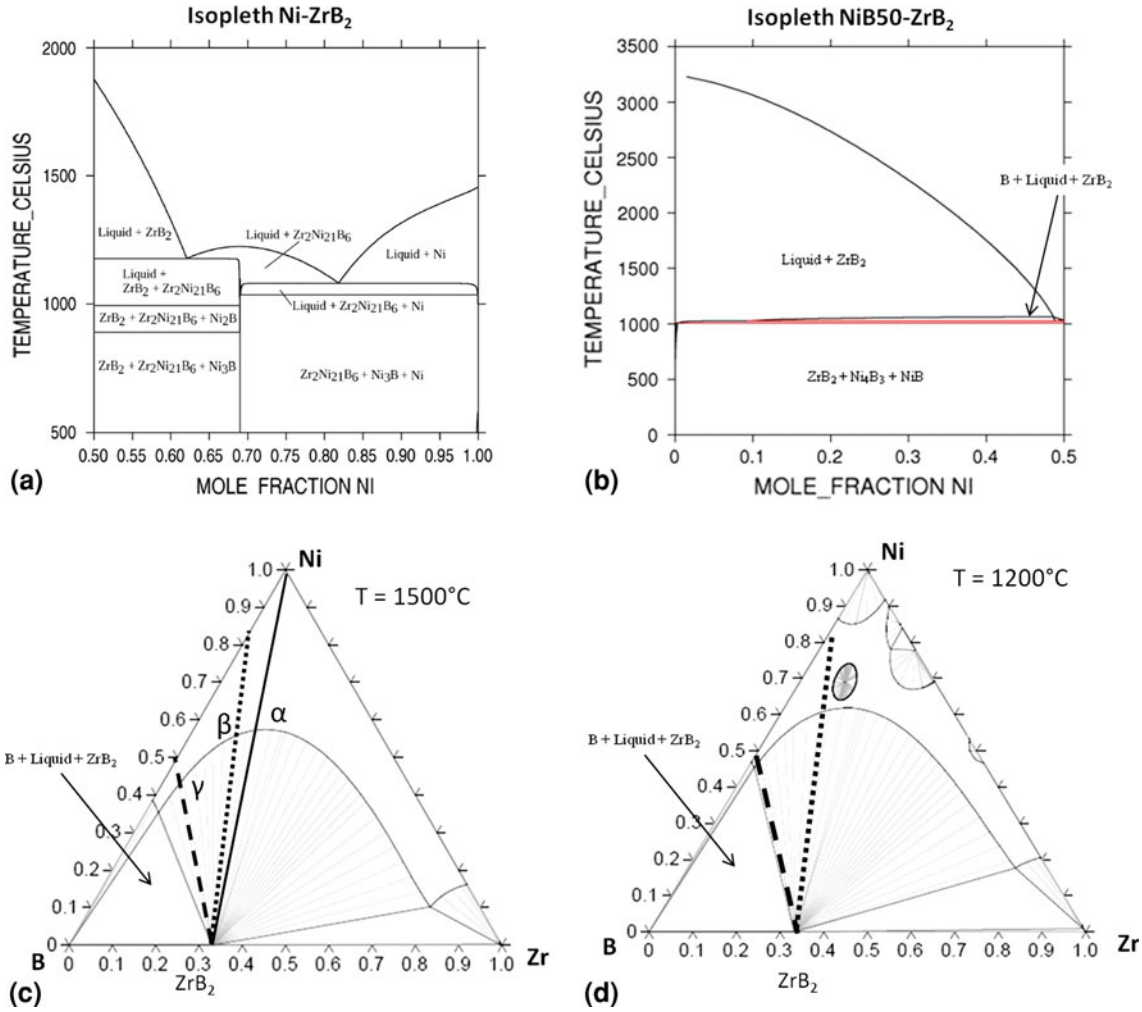

Fig. 6 Calculated B-Ni-Zr phase diagram: (a) Ni-ZrB_2 isopleth; (b) NiB50-ZrB_2 isopleth; (c) isothermal section at 1500 °C; (d) isothermal section at 1200 °C

composition of the liquidus at 1500 °C becomes poorer in Ni (points β and γ, respectively).

For these reasons, remarkable amounts of recrystallized ZrB_2 can be found in the solidified Ni drop, while smaller amounts are present in NiB17 and NiB50.

According to the phase diagram, at 1500 °C a triphasic region exists close to the boron corner, where B, ZrB_2, and a liquid phase coexist. On lowering the temperature, this region widens reaching the composition NiB50 just below 1100 °C: for this reason, boron crystals can be found in the NiB50-solidified drop. This explanation comes also from the NiB50-ZrB_2 isopleth (Fig. 6b) where a narrow region of coexistence of liquid + B + ZrB_2 is depicted. The same isopleth shows that, as revealed by microanalysis, the $Zr_2Ni_{21}B_6$ compound cannot exist and that the solidification leads to a Ni-B alloy and recrystallized ZrB_2.

3.2 Wetting at 1200 °C

Wetting tests have also been performed at 1200 °C with NiB17 and NiB50; the final contact angles are 21° and 58°, respectively.

The NiB17 spreading kinetics (Fig. 7) shows a decrease in contact angles, which occurs in several steps, and the process does not stop even after 25 min from the beginning of the test. At the same time, the drop base diameter grows, and the height decreases.

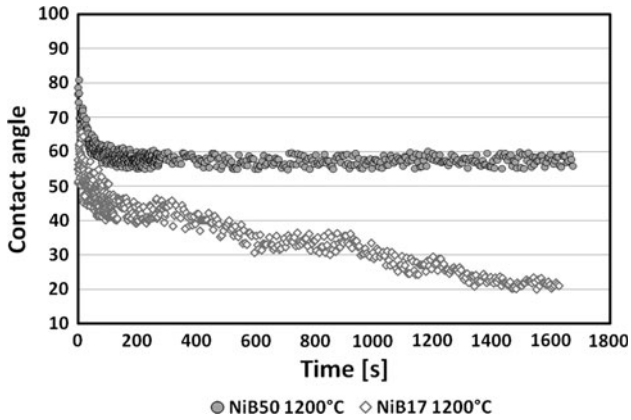

Fig. 7 Kinetics of wetting of the NiB17 and NiB50 at 1200 °C

On the contrary, the spreading of the molten NiB50 alloy takes place in 200 s, and afterward the contact angles do not show any further variation.

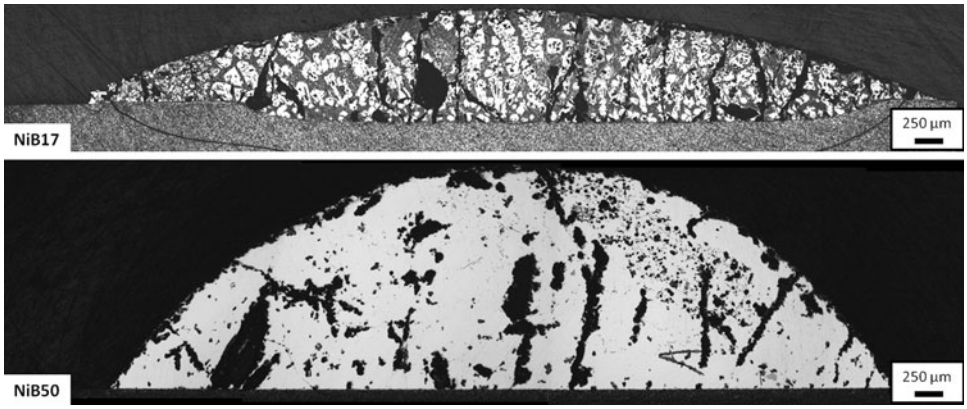

Fig. 8 Optical microscope (OM) pictures of the cross sections of NiB17/ZrB_2 and NiB50/ZrB_2 samples after test at 1200 °C

Cross sections of the NiB17/ZrB_2 and NiB50/ZrB_2 couples are shown in Fig. 8: while the former shows a sigmoidal shape, meaning that an interaction between alloy and ceramics occurs, the resulting NiB50/ceramic interface is macroscopically planar. Again, the microanalyses show the formation of an eutectic structure of the metallic phase for the NiB17 alloy with formation of the compound $Zr_2Ni_{21}B_6$ and introduction of Si into the alloy.

At a microscopic level, the EDS analyses, performed on the NiB50 drop after the wetting test, demonstrate the absence of Zr in any of the spots identified in the solidified alloy, confirming that no dissolution of ZrB_2 occurs at all. Even in this case, pure boron recrystallizes in the metal phase during cooling. Despite the absence of dissolution of the substrate, an eutectic structure is still present caused by a preponderant Ni-B phase accompanied by a primary-solidification phase Ni-Si-B, containing a considerable amount of Si (up to 20 at.%), which, originally located in ZrB_2 grain boundaries, diffuses into the liquid alloy.

According to the isothermal section at 1200 °C of the phase diagram (Fig. 6d), the dissolution of ZrB_2 into the molten alloy is more pronounced for NiB17 than for NiB50 (where it almost disappears), and less pronounced at 1200 than at 1500 °C for both alloys.

The NiB50 alloy showed the highest final contact angles toward ZrB_2: 30° and 58° at 1500 and 1200 °C, respectively.

The amount of Zr introduced in the alloy by the dissolution of ZrB_2 is the key parameter for the explanation of the different wetting behaviors.

It has been demonstrated (Ref 25) that Ag and AgCu alloys, which do not wet pure ZrB_2 (θ [Gt] 90°), show a good wetting behavior when alloyed with Zr. The adsorption at the solid-liquid interface of this active element causes the decrease of the interfacial tension, and thus of the contact angle. This phenomenon is preponderant if compared with the concurrent phenomena occurring at the liquid-vapour surface. Indeed, the Zr dissolution should increase the liquid surface tension of pure Ni, while, simultaneously, B and Si can segregate to the metal surface and lower its surface tension as shown for Cu-B (Ref 40) and Si-Ni alloys (Ref 41), with an effect on the contact angle.

4. Conclusions

The wettings of ZrB_2 by Ni and Ni-B alloys (17 and 50 at.%) were evaluated at 1500 and 1200 °C, by means of the sessile drop method. Wetting results and microstructures were discussed and, coupled with the ternary B-Ni-Zr phase diagram, ad hoc calculated by the CALPHAD method. Even though the fast cooling used in this study led to non-equilibrium solidification conditions, the phase diagram is an extremely useful tool to interpret the phenomena occurring during the metal-ceramic contact.

At 1500 °C, pure Ni wetted well and fast ZrB_2 ($\theta < 10°$), but strong dissolution of the ceramic occurred, accompanied by the dissolution of B, Zr, and Si into the liquid alloy with reprecipitation of ZrB_2 crystals upon cooling and formation of the $Zr_2Ni_{21}B_6$ compound. The dissolution and the following spreading of the saturated alloy led to the characteristic sigmoidal shape of the metal/ceramic interface; moreover, an infiltrated layer formed. As predicted by the phase diagram, the addition of B leads to a decrease (NiB17 alloy) and, finally, to almost the disappearance of the substrate dissolution (NiB50 alloy).

Experiments conducted at 1200 °C showed a decrease in wettability for both the NiB17 ($\theta = 21°$) and NiB50 ($\theta = 58°$) alloys. According to the microanalysis and to the phase diagram, a slight dissolution is still found for the NiB17 alloy, while it is eliminated for the NiB50 alloy.

Compounds such as $ZrSi_2$ and a B-N-O-Si-Zr glassy phase mainly located at the grain-boundary triple lines, which derived from Si_3N_4 used as a sintering enhancer, introduced Si from the ceramic into the liquid phase leading to a quaternary alloy Ni-B-Zr-Si.

Both the wetting behaviors of the ZrB_2 ceramic with Ni and Ni/B alloys and the B-Ni-Zr phase diagram are very similar to those which were found for HfB_2 ceramics and for the B-Hf-Ni system (Ref 29).

Acknowledgments

The authors are grateful to Oskar Ogor (Freie Univers. Berlin) for his help in experimental study. This research is part of the Project "Join*HT*" funded by the "CARIPLO Funding Scheme—2010". The ZrB_2 ceramics were supplied by CNR-ISTEC of Faenza, Italy.

References

1. W.G. Fahrenholtz, G.E. Hilmas, I.G. Talmy, and J.A. Zaykoski, Refractory Diborides of Zirconium and Hafnium, *J. Am. Ceram. Soc.*, 2007, **90**, p 1347–1364

2. S.R. Levine, E.J. Opila, M.C. Halbig, J.D. Kiser, M. Singh, and J.A. Salem, Evaluation of Ultra-High Temperature Ceramics for Aeropropulsion Use, *J. Eur. Ceram. Soc.*, 2002, **22**(14), p 2757–2767
3. A. Bellosi, S. Guicciardi, V. Medri, F. Monteverde, D. Sciti, and L. Silvestroni, Processing and Properties of Ultra-Refractory Composites Based on Zr- and Hf-Borides: State of the Art and Perspectives, Phys. and Astronomy, *Boron Rich Solids*, N. Orlovskaya and M. Lugovy, Ed., Springer, 2011, p 147–160
4. G.V. Samsonov, A.D. Panasyuk, and M.S. Borovikova, Study of the Wetting of Metal like Borides by Liquid Metals, *Poroshkovaya Metallurgiya*, 1973, **5**, p 61–67 (in Russian)
5. G.V. Samsonov, A.D. Panasyuk, and M.S. Borovikova, Reaction Between Refractory Diborides and Liquid Iron Group Metals, *Poroshkovaya Metallurgiya*, 1973, **6**, p 51–57 (in Russian)
6. V.I. Tumanov, A.E. Gorbunov, and G.M. Kondratenko, Wetting and Properties of Group IV and VI, Metal Mono- and Di-Borides, *Russ. J. Phys. Chem.*, 1970, **44**, p 304 (in Russian)
7. G.V. Samsonov, O.P. Sharkin, A.D. Panasyuk, and L.V. D'yakonova, Electron Microprobe Investigations of Interfacial Reactions in Systems Composed of a Refractory Compound and a Liquid Metal, *Poroshkovaya Metallurgiya*, 1974, **7**, p 63–68 (in Russian)
8. V. Ukov, O.A. Esin, H.A. Vatolin, and E.L. Dubinin, Investigation of Wetting of Non-Metallic Solids by Pd-Based Liquid Alloys, *Physical Chemistry of Surface Phenomena at High Temperature*, V.N. Eremenko, Ed., Naukova Dumka, Kiev, 1971, p 139–146
9. A. Passerone, M.L. Muolo, F. Valenza, F. Monteverde, and N. Sobczak, Wetting and Interfacial Phenomena in Ni-HfB_2 Systems, *Acta Mater.*, 2009, **57**(2), p 356–364
10. A. Passerone, F. Valenza, and M.L. Muolo, Transition Metal Diborides: From Wettability to Brazing, *J. Adhes. Sci. Technol.*, in press
11. M.L. Muolo, F. Valenza, N. Sobczak, and A. Passerone, Overview on Wetting and Joining in Transition Metals Diborides, *Adv. Sci. Technol.*, 2010, **6**, p 98–107
12. X. Zhang, C. Hong, J. Han, and H. Zhang, Microstructure and Mechanical Properties of TiB_2/(Cu, Ni) Interpenetrating Phase Composites, *Scripta Mater.*, 2006, **55**(6), p 565–568
13. J.S. Gam, K.S. Han, S.S. Park, and H.C. Park, Joining of TiB_2-Al_2O_3 Using Compositionally Graded Interlayers, *Mater. Manuf. Proc.*, 1999, **14**(4), p 537–546
14. Y. Peng, Z.Y. Fu, W.M. Wang, H. Wang, Y.C. Wang, J.Y. Zhang, and Q.J. Zhang, Joining TiB_2-Ni Cermets with Ti6Al4V by Pulse Current Heating, *Key Eng. Mater.*, 2008, **368**, p 1609–1611
15. J.H. Yun, J.H. Kim, J.S. Park, Y.D. Park, Y.H. Park, K.M. Cho, and I.M. Park, Properties of Cu-TiB_2 Composites Fabricated by In Situ Liquid Melt Mixing Process, *Adv. Mater. Res.*, 2006, **15–17**, p 215–219
16. M.L. Muolo, E. Ferrera, L. Morbelli, C. Zanotti, and A. Passerone, Joining of Zirconium Boride Based Refractory Ceramics to Ti6Al4V, *Proceedings of the 9th International Symposium on Materials in a Space Environment*, K. Fletcher, Ed., Jun 16–20, 2003 (Noordwijk, The Netherlands), European Space Agency ESA SP 540, 2003, p 467–472
17. A. Passerone, M.L. Muolo, L. Morbelli, E. Ferrera, M. Bassoli, and C. Bottino, Joining of Bulk Refractory Ceramics: Interactions, Wetting and Interfacial Structures, *Proceedings of the 4th European Workshop Hot Structures and Thermal Protection Systems for Space Vehicles*, A. Wilson, Ed., Nov 26–29, 2002 (Palermo, Italy), European Space Agency ESA SP-521, 2003, p 295–301
18. M. Singh and R. Asthana, Joining and Integration of ZrB_2-Based Ultra-High Temperature Ceramic Composites Using Advanced Brazing Technology, *J. Mater. Sci.*, 2010, **45**, p 4308–4320
19. R. Asthana and W. Singh, Joining of ZrB_2-Based Ultra-High-Temperature Ceramic Composites Using Pd-Based Braze Alloys, *Scripta Mater.*, 2009, **61**, p 257–260
20. M. Singh and R. Asthana, Joining of Zirconium Diboride-Based Ultra High-Temperature Ceramic Composites Using Metallic Glass Interlayers, *Mater. Sci. Eng. A*, 2007, **460**, p 153–162
21. M. Singh and R. Asthana, Joining of ZrB_2-Based Ultra-High-Temperature Ceramic Composites to Cu-Clad-Molybdenum for Advanced Aerospace Applications, *Int. J. Appl. Ceram. Technol.*, 2009, **6**, p 113–133
22. L. Esposito and A. Bellosi, Joining ZrB_2-SiC Composites Using Glass Interlayers, *J. Mater. Sci.*, 2005, **40**, p 4445–4453
23. W.R. Pinc, M. Di Prima, L.S. Walker, Z. N. Wing, and E. L. Corral, Spark plasma joining of ZrB_2-SiC composites using zirconium-boron reactive filler layers, *J. Am. Ceram. Soc.*, 2011, **94**(11), p 3825–3832
24. N. Sobczak, R. Nowak, A. Passerone, F. Valenza, M.L. Muolo, L. Jaworska, F. Barberis, and M. Capurro, Wetting and Joining of HfB_2 and Ta with Ni, *Trans. Foundry Res. Inst.*, 2010, **2**, p 5–14
25. M.L. Muolo, E. Ferrera, R. Novakovic, and A. Passerone, Wettability of Zirconium Diboride Ceramics by Ag, Cu, and Their Alloys with Zr, *Scripta Mater.*, 2003, **48**, p 191–196
26. M.L. Muolo, E. Ferrera, and A. Passerone, Wetting and Spreading of Liquid Metals on ZrB_2-Based Ceramics, *J. Mater. Sci.*, 2005, **40**, p 2295–2300
27. A. Passerone, M.L. Muolo, and D. Passerone, Wetting of Group IV Diborides by Liquid Metals, *J. Mater. Sci.*, 2006, **41**, p 5088–5098
28. G. Cacciamani, P. Riani, and F. Valenza, Equilibrium Between MB_2 (M = Ti,Zr,Hf) UHTC and Ni: A Thermodynamic Database for the B-Hf-Ni-Ti-Zr System, *CALPHAD*, 2011, **35**(4), p 601–619
29. L. Kaufman, G. Cacciamani, M.L. Muolo, F. Valenza, and A. Passerone, Wettability of HfB_2 by Molten Ni(B) Alloys Interpreted by CALPHAD Methods. Part 1: Definition of the B-Hf-Ni System, *CALPHAD*, 2010, **34**, p 2–5
30. A. Passerone, M.L. Muolo, F. Valenza, and L. Kaufmann, Wettability of HfB_2 by Molten Ni(B) Alloys Interpreted by CALPHAD Methods. Part 2: Wetting and Interfacial Reactivity, *CALPHAD*, 2010, **34**, p 6–14
31. A. Passerone, M.L. Muolo, R. Novakovic, and D. Passerone, Liquid Metal/Ceramic Interactions in the (Cu, Ag, Au)/ZrB_2 Systems, *J. Eur. Ceram. Soc.*, 2007, **27**, p 3277–3285
32. H.H. Stadelmaier and B.B. Helms, Ein Borid mit $Cr_{23}C_6$-Struktur im System Nickel-Zirkon-Bor, *Metall*, 1965, **19**, p 121–122 (in German)
33. Y.V. Voroshilov and Y.B. Kuz'ma, The Systems Zirconium-Nickel-Boron, *Soviet Powder Metall. Met. Ceram.*, 1967, **9**, p 17–20 (in Russian)
34. E. Lugscheider, H. Reimann, and R. Pamkert, Mit 4a- und 5a-Metallen stabilisierte tau-Boride des Nickel, *Metall*, 1982, **36**, p 247–251 (in German)
35. F. Monteverde, S. Guicciardi, and A. Bellosi, Advances in Microstructure and Mechanical Properties Of Zirconium Diboride Based Ceramics, *Mater. Sci. Eng. A*, 2003, **346**, p 310–319
36. N. Eustathopoulos, M.G. Nicholas, and B. Drevet, *Wettability at High Temperatures*, Pergamon Materials Series, Pergamon, Oxford, 1999
37. L. Liggieri and A. Passerone, An Automatic Technique for Measuring the Surface Tension of Liquid Metals, *High Temp. Technol.*, 1989, **7**, p 80–86
38. F. Valenza, M.L. Muolo, and A. Passerone, Wetting and Interactions of Ni- and Co- Based Superalloys with Different Ceramic Materials, *J. Mater. Sci.*, 2010, **45**(8), p 2071–2079
39. N. Eustathopoulos, N. Sobczak, A. Passerone, and K. Nogi, Measurement of Contact Angle and Work of Adhesion at High Temperature, *J. Mater. Sci.*, 2005, **40**(9–10), p 2271–2280
40. A. Passerone, M.L. Muolo, F. Valenza, and R. Novakovic, Thermodynamics and Surface Properties of Liquid Cu-B Alloys, *Surf. Sci.*, 2009, **603**, p 2725–2733
41. G.W. Liu, M.L. Muolo, F. Valenza, and A. Passerone, Survey on Wetting of SiC by Molten Metals, *Ceram. Int.*, 2010, **36**, p 1177–1178